Self-Sustaining Wireless Communication Networks

Kozhakhmet Abdugapbar, Master in Electrical and Computer Engineering

Submitted in fulfilment of the requirements for the degree of Master of Science in Electrical and Computer Engineering

NAZARBAYEV UNIVERSITY

School of Engineering and Digital Sciences

Department of Electrical and Computer Engineering

Nazarbayev university

53 Kabanbay Batyr Avenue,

Astana, Kazakhstan, 010000

Supervisors: Dr. Mohammad Hashmi, Dr. Galymzhan Nauryzbayev

April 2024

Declaration

I hereby, declare that this manuscript, entitled “Development of a Smart Reflective Surface-enabled System for Wireless Networks”, is the result of my own work except for quotations and citations which have been duly acknowledged.

I also declare that, to the best of my knowledge and belief, it has not been previously or concurrently submitted, in whole or in part, for any other degree or diploma at Nazarbayev University or any other national or international institution.

(Signature of author)

Name:

Date:

Abstract

The increasing demand for wireless communication systems and the associated challenges of maintenance costs and environmental impact arise the need for sustainable and efficient energy sources. This work is about designing an RF energy harvesting system for wireless communication networks. The metamaterial (MTM) absorbers were selected as the main components of the RF system. MTM absorbers have unique properties and near-ideal absorption, which makes them good candidates for energy harvesting. The MTM absorbers were studied in a literature review to select the best fundamental structure for a unit cell. The absorber was designed and simulated using a CST simulator and operated at 29.5 GHz. The simulation results show good absorption rates and impedance matching between the ports. The experimental setup was built to test the manufactured design. The setup consisted of an anechoic chamber, signal generator, horn antenna, RF cables, a 3D model of the stand, a spectrum analyzer, and an MTM absorber. A power budget was calculated to not damage the equipment and compare input and output results. The results of the experimental measurements were analysed and compared with the simulation results.

Acknowledgements

I would like to thank the professors who supported and guided me during my thesis project. My supervisor, Dr. Mohammad Hashmi, and co-supervisor, Dr. Galymzhan Nauryzbaev, provided me with an opportunity to deepen my knowledge of wireless communication and gave me experience working with various equipment in the lab. In addition, I would like to express my gratitude to my family members and loved ones for creating an environment where I can effectively study and work.

Table of Contents

List of Abbreviations

MTM	Metamaterial
RF	Radio Frequency
UC	Unit Cell

List of Tables

List of Figures

Chapter 1 – Introduction

1.1 Background

The growth of wireless technology in the modern world creates new opportunities and challenges at the same time. Wireless communication systems installed in houses and workplaces help to save time and become more efficient [1]. However, there are some difficulties with the cost of maintenance. Most of the systems operate with the help of sensors and small devices used for data gathering and operation. Most of them are powered by batteries, which may be ineffective and problematic as it requires time and sometimes effort to replace them regularly. The environmental effect of lithium batteries that are commonly used is huge [2].

There are renewable, environmentally friendly energy sources that can be used to power communication system devices. One of the most efficient energy sources is solar energy. It is already widely used to power lamps and outdoor devices by installing solar panels on them. The efficiency of the panels is determined by sunlight and the material of the panels [3]. Nevertheless, there are a number of disadvantages to using solar energy for indoor energy collection. First off, indoor lighting is far less intense than direct sunlight, which lowers the efficiency of power generation. Due to this restriction, larger or more effective PV panels are needed to produce enough power, which can be difficult in an indoor environment with limited space [4]. Second, irregular energy supply may result from indoor lighting circumstances that are unpredictable, such as variations in artificial lighting or variations in natural light brought on by the time of day and the weather. Furthermore, installing PV cells and the related energy management systems can be somewhat expensive initially, but over time, lower energy costs more than make up for this. Lastly, because PV panels must be installed in well-lit places for optimal energy collection, which may

not always coincide with interior design preferences, the aesthetic integration of PV panels into indoor spaces can be problematic.

Mechanical vibrations are another way that wireless communication devices can be powered in an indoor environment. Piezoelectric disks are thin, circular pieces composed of materials that have the ability to convert mechanical strain into electrical energy and vice versa. Examples of these materials include quartz and certain ceramics [5]. These disks are frequently utilized in many different applications, such as energy harvesting devices, actuators, and sensors. Piezoelectric disks are used in energy harvesting to extract energy from mechanical vibrations in the surrounding environment, including those caused by machinery, structural motions, and even human activity. The piezoelectric effect causes these disks to produce an electrical charge when they are subjected to mechanical stress or vibrations. Piezoelectric energy harvesting is a viable alternative for self-powered sensors and wireless devices in remote or inaccessible locations since this electrical energy can be saved or used to power low-energy electronic devices [6]. Because piezoelectric materials are durable, this strategy ensures low maintenance and long-term reliability by reducing dependency on external power sources and batteries. The method does, however, have certain drawbacks, including a lower power output, uneven energy generation based on vibrations in the surrounding environment, and higher startup expenditures in comparison to conventional power sources. Furthermore, the availability of appropriate mechanical vibrations is a condition for the success of piezoelectric energy harvesting, which may not be present in every indoor environment. They can be set in places where lots of people pass, like aisles and corridors, to optimize the energy output.

This study suggests radio frequency (RF) energy harvesting as a way to recharge batteries and make communication systems self-sustaining. This technique is particularly effective in interior situations where there are many RF sources, such as Wi-Fi routers, Bluetooth devices, and

cellular signals [7]. With the use of antennas and rectifiers, these widespread signals can be harvested by RF energy harvesters and converted into a small but reliable power source. RF energy harvesting becomes an intriguing option for powering low-energy devices like wearable technology, wireless sensors, and Internet of Things devices since it does away with the need for batteries and other external power sources [8]. The metamaterial (MTM) absorber is one of the most promising absorber types for RF energy harvesting. These absorbers are designed to achieve near-perfect absorption of electromagnetic waves, such as microwaves, terahertz waves, and visible light, over a specific frequency range. By modifying the geometry and composition of the resonant parts, MTM absorbers can be specifically tuned for various applications [9]. This makes it possible to produce absorbers with extremely selective frequency responses, which is advantageous for uses in energy harvesting, sensing, and stealth technologies. Furthermore, these material's thin and light weight make them desirable for incorporation into a variety of surfaces and devices.

2.1 Literature Review

Wireless communication network development is essential in the modern era, where information transfer is important. The research team at the University of Technology in Vienna built a system that uses energy from solar cells and vibrations. The harvested energy was stored in small capacitors and used to power a 100–200 μW sensor node [10]. RF energy harvesting was also implemented to capture and store energy coming from the transmitter antenna. In the Figure 1, a far-field wireless power transfer energy transfer architecture is proposed [11]. The RF wave is captured by a rectenna antenna. Then, it is measured with an impedance matcher to have low power loss. The voltage multiplier converts AC power to high DC power. The energy is stored in capacitors for further use. However, the RF energy harvesting system produces far less power than solar or mechanical methods. This type of system can be implemented on low-power devices that are frequently used in Internet-of-Things networks.

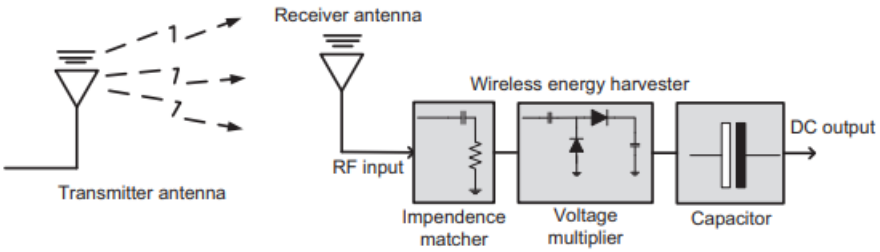

Figure 1. Far-field wireless power transfer [11].

There is an implementation of several energy sources into one power system for better output power [12]. The Figure 2 shows the general system with energy sources, converters, and a powered sensor. There are thermal, solar, vibrational, and RF energy sources combined to transfer energy into the power system. The power system includes converters, energy storage, and power management devices. The converted energy goes to power sensors or other low-power devices.

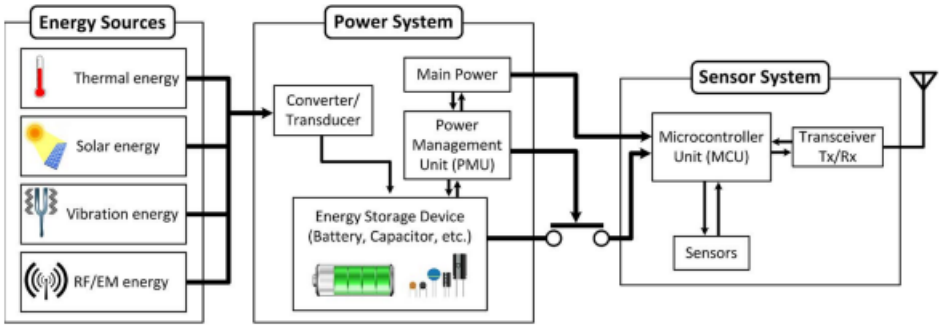

Figure 2. Block diagram of the energy harvesting system for powering sensors [12].

There are many conditions that affect the efficiency of energy harvesting systems. The most common one is the weather conditions that affect the performance of solar energy. The optimal placement, panel choice, and size must be optimized to obtain maximum harvested energy at a lower cost [13]. The main difficulty with RF energy harvesting is the low power and lack of line of sight between potential RF sources and absorbers or antennas. The research about nonlinear far-field RF energy harvesting studied real, theoretical, linear, and nonlinear models [14]. The

experimental linear and nonlinear models do not match theoretical values. With the increase in input power, the harvested energy linearly rises until it reaches saturation.

RF energy harvesting needs an efficient antenna or absorber to harvest electromagnetic waves effectively. In this case, developing MTM absorbers for energy harvesting has attracted many researchers. Most of the MTM designs achieved high absorption rates. MTM is a unique material with properties like negative permeability and permittivity [15]. The common design of the MTM absorber consists of dielectric material, ground, and metal patterns [16], [17]. The metallic pattern on the top of the substrate can be changed to obtain certain frequencies and absorption rates. One of the fundamental designs of the absorber is the square split-ring resonator on top of the substrate [18]. Figure 3 presents the design of the MTM absorber designed to operate at 2.8 GHz, 5.4 GHz, and 10.5 GHz. The gap between rings, the thickness of the metallic line, and the length of the pattern define its absorption rate and frequency. The three layers of resonators resulted in absorption at three frequencies with 80%, 90%, and 85% efficiency.

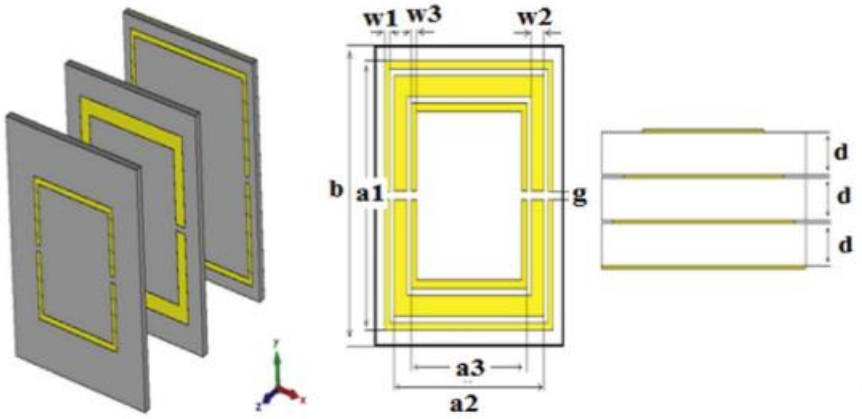

Figure 3. The multi-layered absorber structure for energy harvesting purposes [18].

Another split-ring multiband absorber was developed to work at several frequencies for better energy harvesting properties [19]. It explains that radio frequency energy harvesting is a reliable way to power electronic systems compared to other sources because of the dense radio

frequency environment. It compensates for the low power of radio frequencies with a great number of sources. The proposed absorber is made to resonate in specific frequency bands, such as LTE 2350, Wi-Fi 2450, and LTE 2600, and tuned by performing parametric analysis. The important parameters of the design were altered and observed to provide the most efficiency at the needed frequency. The design is simulated using Ansys HFSS software, and the results show that the antenna resonates at the three frequencies with a return loss of −15 dB, −28 dB, and −27 dB. The compact structure size of 35 mm x 35 mm x 1.67 mm makes it easy to implement them on different surfaces without harming the view or aesthetics. The great absorption rate was achieved due to the split ring pattern. Additionally, several rings provide absorption at three frequencies, making the absorber a multiband one. Another absorber design includes a Schottky diode across the gap of the split-ring resonator [20]. The purpose of the diode is to create DC voltage by rectifying resonant current excited by RF waves. The study introduces a metasurface in the shape of an ”L” designed for radio frequency energy harvesting [21]. This metasurface comprises unit cells (UCs), each adorned with four ”L”-shaped patterns. In simulation, the proposed metasurface exhibited a noteworthy 90% absorption rate at 2.25 GHz. Importantly, the absorber maintained stability when exposed to incident angles as high as 50 degrees. The authors performed experiments to check the efficiency of energy harvesting metasurfaces. They connected several UCs and produced waves from the signal generator. Then, using diodes, UC output was connected and measured using a voltmeter. This provided a real efficiency of 55%, which is less than the simulation.

This paper presents a rectangular-shaped MTM absorber based on a multi-layered square split ring structure [22]. The proposed design has good absorption and polarization and is independent of the incident angle. Unlike the other papers, this absorber works at several frequencies and has wideband characteristics as well. The impact of parameters, material choice, and incident angle was examined by printing out the design and performing experimental

validation. The absorption level varied between 70% and 99%. As a result, the absorption and operating frequencies do not depend much on the incident angle, which makes the proposed design a good candidate for energy harvesting devices.

The MTM absorber was designed to operate at a wideband frequency [23]. The three-layer MTM absorber design has light PVC, aluminum, and conductive PLA. The device presented a more than 80% absorption rate between 7 GHz and 13 GHz. The angle sensitivity was also evaluated and simulated at various polarization angles. There is a frequency shift and slight absorption degradation during the increase in the incident angle. The reason for the great angle sensitivity is the flexibility of the material. The measurement setup includes two horn antennas and a vector network analyzer. The advantages of this type of MTM absorber are its high absorption rate at different polarization angles and flexibility. The flexible material allows the absorber to be implemented not only on a plane but also on a convex surface as presented in Figure 4.

Figure 4. The flexible MTM absorber for X-band application [23].

Another flexible MTM absorber was designed with two layers of substrate and six circular patterns [24]. The proposed design resulted in three absorption rates of 96.91%, 96.41%, and 90.12% at 1.75, 2.17, and 2.6 GHz. For the experimental verification, an array of 4×4 with 16 UCs was fabricated. Furthermore, the experimental measurement was done by the waveguide port that

is presented in Figure 5. For better energy harvesting, the loads were implemented in circular metallic patterns. The numerical values of loads were estimated from the input impedances.

Figure 5. The waveguide measurement method arrangement [24].

The research on the step-by-step design of the MTM unit cell was presented [25]. The initial design of the unit cell consists of a single square ring with one gap. Furthermore, the design was developed for the square ring with the hexagonal structure inside of it. This development resulted in a frequency shift and improvement of the transmission from -20 dB to -30 dB. The MTM property extraction was done, and the results provided single-negative MTM.

The operating frequency of the absorber also plays a huge role. The most common frequencies for energy harvesting systems are 2.4 GHz and 5.8 GHz. This is the frequency at which most wireless communication devices operate. However, there is a MTM absorber that works at terahertz frequencies [26]. It is designed to be used in future 6G communication. The size of the UC is very small, 33 μm by 33 μm.The design shows almost perfect absorption at 0.89 THz and 1.36 THz. The experimental measurement was completed using a terahertz TDS system.

1.3 Aims and Objectives

MTM absorbers can be part of the energy harvesting system for the wireless communication system. The main concern about them is the efficiency of the energy harvesting, as RF waves produce less energy. To compensate for this drawback, the MTM absorber should have nearly perfect absorption levels.

This research aims to implement an efficient MTM absorber design and experimentally verify it. The main research objectives are:

- to do research on creating a unique UC absorber design.
- to simulate the proposed design using various RF simulators.
- to implement the UC design into an array of MTM absorbers to measure output power.
- to construct a measurement setup that eliminates noise and gives the opportunity to test power efficiency.
- to test and measure the printed MTM absorber using an experimental setup.
- to compare simulation and experimental results to verify the MTM absorber design.

1.4 Thesis Structure

This project will start with reading and studying existing literature about MTM absobers in wireless communication. The methods of efficiently designing a MTM absorber and tuning it will be obtained. Then the simulation process will be studied. The various port configurations and simulation programs need to be used to verify the design before manufacturing. The most common programs that are used are CST Simulator and HFSS Ansys. The experimental validation will require additional hardware like a vector network analyzer, SMA ports, cables, an ocsiloscope, horn antennas, and a signal generator. It will be better if an anechoic chamber is used to avoid any noise in the results.

Chapter 2 – Method development

2.1 Unit Cell Design

The UC is the fundamental part of any periodic structure. The parameters of UC determine the performance and characteristics of the device. The first step in designing a MTM absorber is to create an efficient UC that works at a desirable frequency. The analysis of previous works provided a template for creating an absorber design. The substrate material for the absorber was Rogers 4350B material, with a dielectric constant of 3.66 and a loss tangent of 0.0037. Then another layer of FR-4 substrate was added to connect the microstrip line to the absorber. Two layers of substrate and top and bottom copper layers were connected via. There is a ground between two dielectrics to prevent the impact of each layer on another. The proposed design of the absorber is presented in Figure 6. The size of the unit cell is 8 mm × 8 mm. The gaps at the sides of the rectangular ring concentrate the current density and the reason for the absorption. The split-ring-resonator concept was taken as a fundamental for the proposed UC. Overall, the absorber will be light, compact, and small, which means that it can be fitted and installed on any small surface or device. Furthermore, the 13 × 11 unit cell array was constructed using UC design.

The UC design was completed through a step-by-step evaluation of performance. The first UC design consisted of a square-ring resonator. It was based on the structures of papers reviewed earlier. The gap between two rings produces the capacitance at the edges, as presented in Figure 6a. The following design was needed to observe absorption at some frequency. Furthermore, the line between two split rings was introduced, as depicted in Figure 6b. It was done to increase the area of copper and obtain higher absorption rates. Then, to tune the frequency of UC, two small lines were added, and the gap distance was changed. By optimizing the paramaters, the final design of UC with high absorption and a suitable operating frequency was achieved in Figure 6c. The

main difficulty was optimizing the design without complicating the pattern. To be able to maintain high absorption and change the operating frequency to desired levels, a lot of tunable parameters are needed. In most cases, a simple square-ring resonator is not enough to increase absorption and shift the frequency within the same size of UC. The parameters of each design are shown in Figure 7. The first design resulted in absorption around 25.9 GHz with a gain of -17 dB. Furthermore, the changes in the second design resulted in a higher absorption rate. The final design was optimized to get even more absorption at higher frequencies. The reason for not stopping at -20 dB gain and increasing it up to -50 dB is that UC will have degradation of absorption when combined into a MTM absorber array.

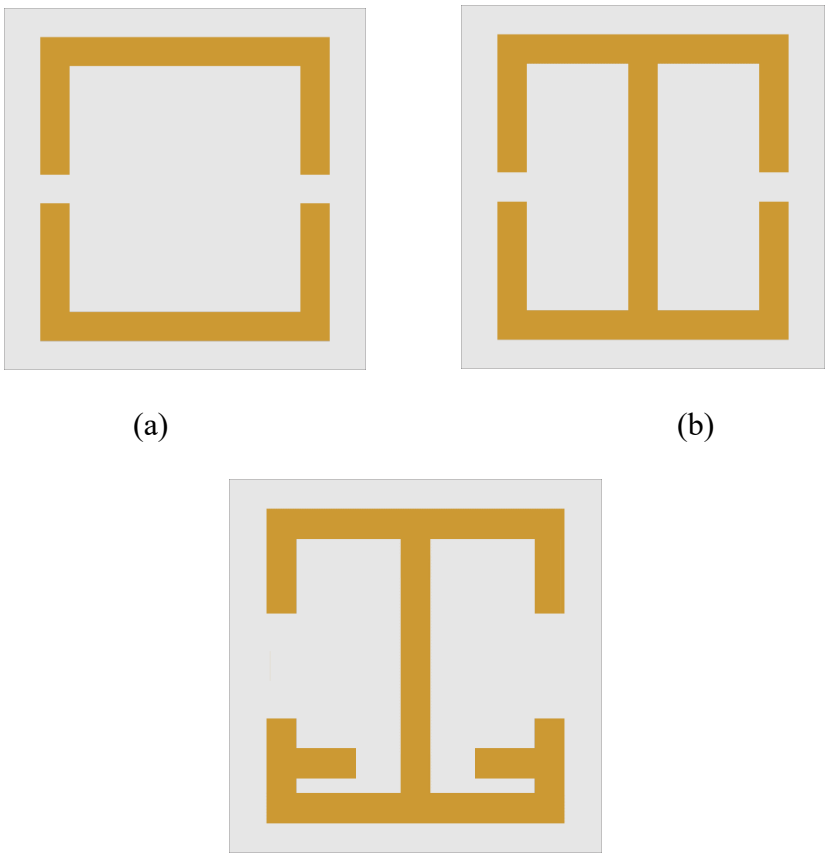

(a) (b)

(c)

Figure 6. UC design of the MTM absorber: (a) first, (b) second, (c) final.

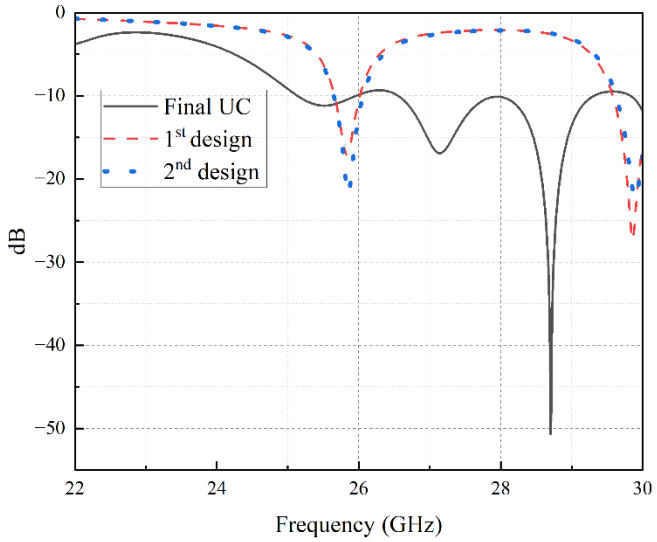

Figure 7. S_{11} changes at each UC design steps.

2.2 Simulation

The absorber was designed and simulated using a CST Simulator. The simulator provides us with a user-friendly interface to build a 3D model of the UC and choose appropriate material from the library. There are two main configurations for simulating periodic structure: floquet port boundaries and waveguide ports. The floquet port boundaries take the UC and simulate it as a periodic structure. The floquet port boundaries are set as “unit cell” and ports are defined in the open space boundary as presented in Figure 8a. The waveguide ports should be defined manually, and the other two axes, rather than ports, are electrical and magnetic boundaries. The distance of waveguide ports is set automatically depending on the side of the UC, like in Figure 8b. One of the ports should be connected to the microstrip line. The second port is built automatically on the face of the microstrip line using the “Solver” command. The floquet port simulates faster, so all design optimization was done on a floquet port configuration. Furthermore, the impedance matching was done using waveguide ports.

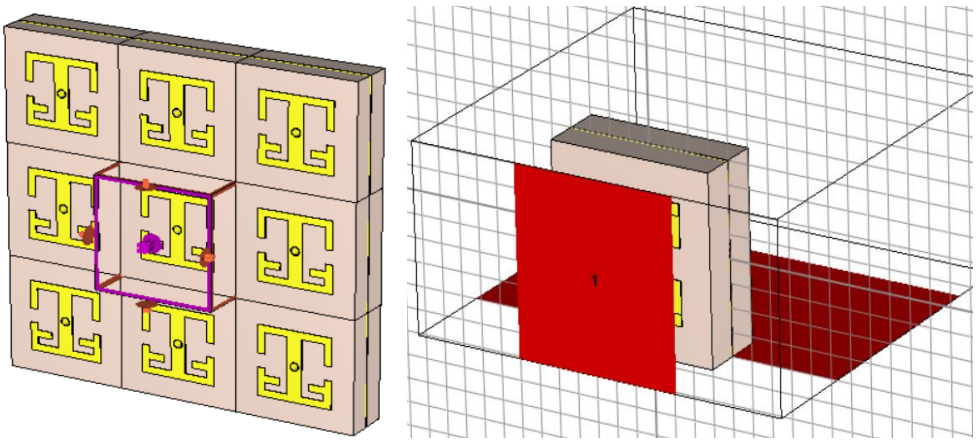

(a) (b)

Figure 8. Simulation configuration: (a) floquet ports, (b) waveguide ports.

Furthermore, UC was simulated using different boundaries to see the difference in S-parameter results. Both configurations resulted in the same graph with approximately the same absorption point. Figure 9a presents the reflection loss of -50.67 dB at 28.7 GHz. The absorption rate is calculated using the equations (1-2) below:

$$A(\omega) = 1 - |S_{21}|^2 - |S_{11}|^2 \quad (1)$$

$$A(\omega) = 1 - |S_{11}|^2 \quad (2)$$

The proposed design has a copper plate at the back of the absorber to equalize the value to zero. This will result in the equation (2) that was used for the calculation of the absorber. According to the calculation, the absorption level is 99.9 % as presented in Figure 9b.

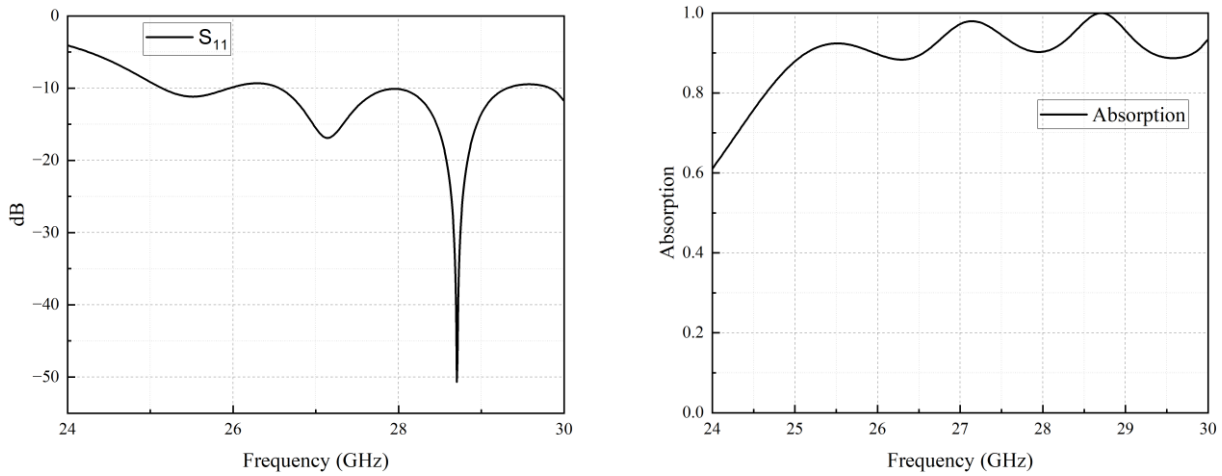

(a) (b)

Figure 9. UC simulation results: (a) S_{11} parameter, (b) absorption.

Furthermore, the MTM properties of UC were examined. It is needed to make sure that the designed absorber exhibits MTM characteristics. The S-parameters obtained from simulation will be used to compute the impedance of the absorber, refractive index, permittivity, and permeability [17]. The equations below were used to compute impedance and refractive index.

$$z = \sqrt{\frac{(1+S_{11})^2 - S_{21}^2}{(1-S_{11})^2 - S_{21}^2}}, \tag{3}$$

$$n = \frac{1}{k_0 l}\left[\left(\left[ln\left(e^{ink_0 l}\right)\right]'' + 2m\pi\right) - i\left[\left[ln\left(e^{ink_0 l}\right)\right]'\right]\right], \tag{4}$$

where k_0 is the wavenumber, l is the length of UC, and m is the branch of periodicity. Furthermore, the calculated refractive index and impedance will be used to determine permittivity (ε) and permeability (μ).

$$\varepsilon = \frac{n}{z}, \tag{5}$$

$$\mu = n * z \tag{6}$$

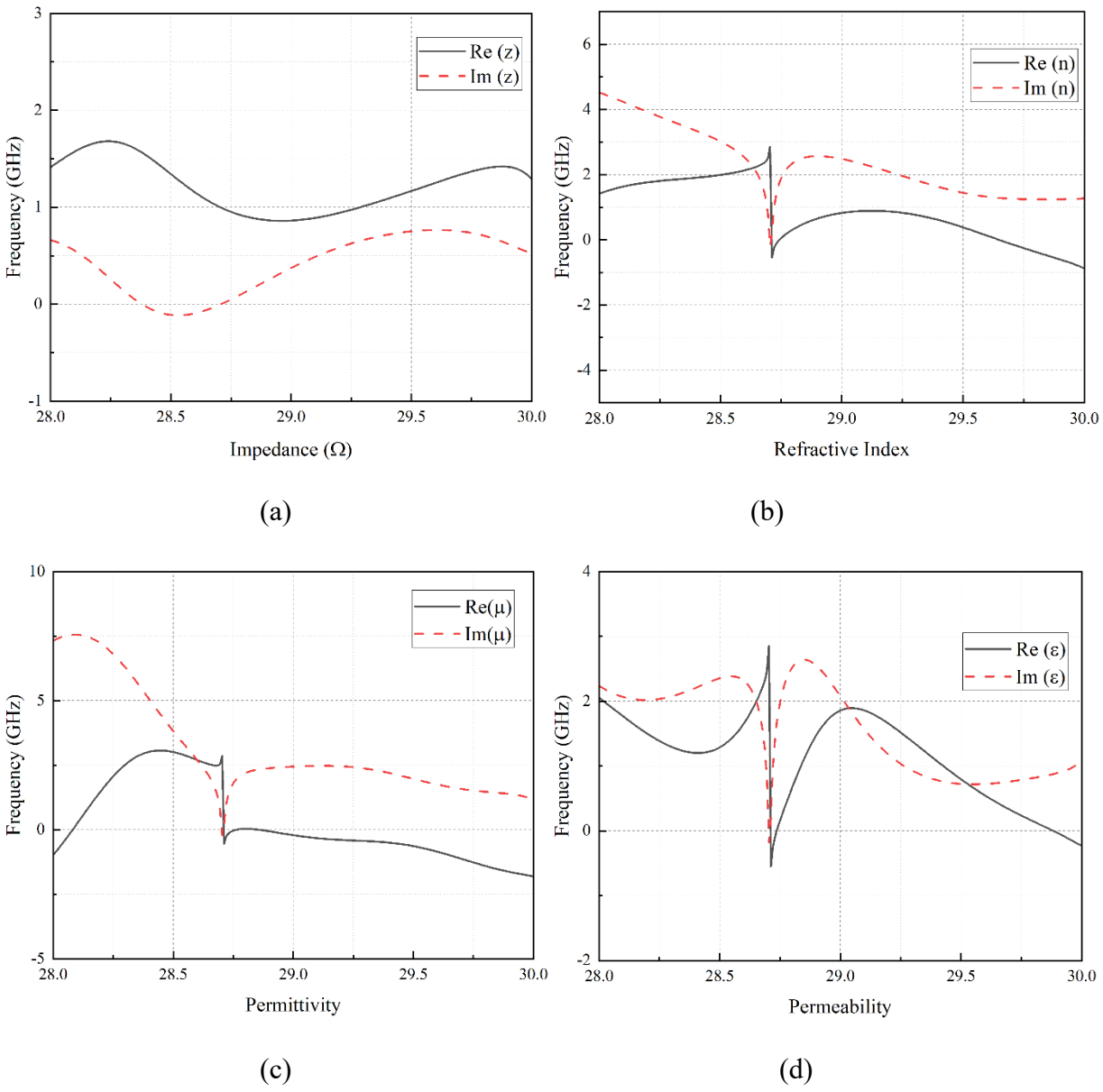

Figure 10. MTM properties of UC: (a) impedance, (b) refractive index, (c) permittivity, (d) permeability.

As it can be seen from Figure 10, the refractive index, permittivity, and permeability are negative at the operating frequency. This proves the double-negative MTM property of the designed UC. After determining all the properties of UC, the MTM absorber array can be built and tested. The negative permittvity and permeability means that the absorber have artificial response as the result of the engineering, not because of the material composition.

The current density distribution of UC was observed from simulation and depicted in Figure 11. The high concentration of current is located between gaps and lower lines. These gaps provide additional capacitance to the MTM absorber. When the absorber is affected by the incident waves, these capacitors store some energy and lead to higher electric strength and higher current density. There is some current density at the edges of the UC which indicates that UCs will affect each other when combined to the array.

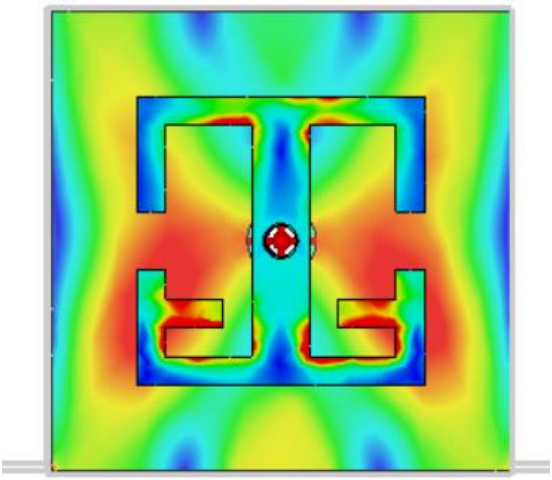

Figure 11. The current density distribution of UC.

2.3 Metamaterial absorber array

Furthermore, the array was simulated by connecting all unit cells into one microstrip line. The scattering parameter of the array is depicted in Figure 12a. In the graph, S_{11} is the reflected wave used to determine absorption, and S_{22} is the scattering parameter of the output port. It can be seen that a frequency shift occurred due to the mutual coupling between the unit cells. However, there is still a -21.75 dB antenna gain that results in a 99% absorption rate as shown in Figure 12b. The S_{22} gain at a working frequency equals -20.17 dB, which means low power loss at the output port. It can be noted. That the S_{22} values are lower than -15 dB at the frequency range of 28 GHz and 30 GHz.

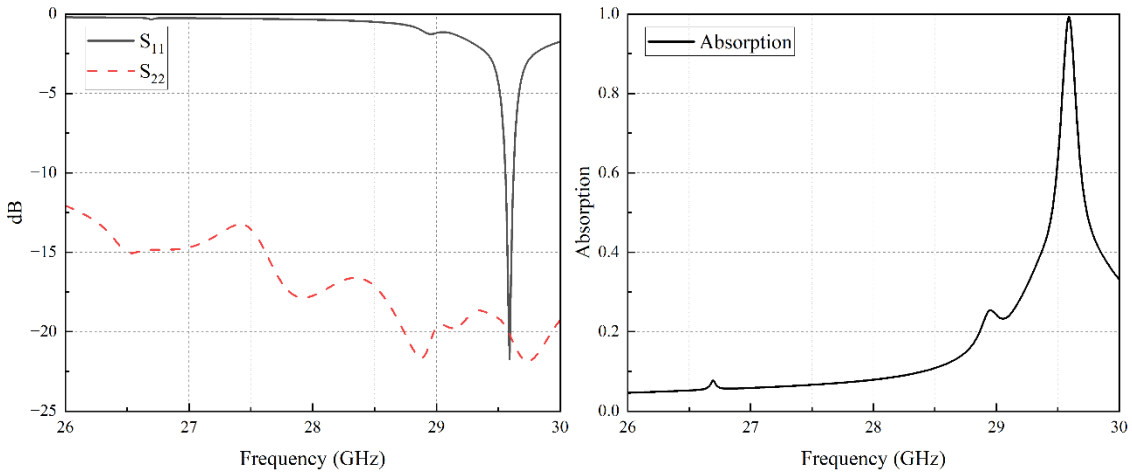

(a) (b)

Figure 12. Simulation results of the MTM absorber array: (a) S-parameters, (b) absorption.

The MTM absorber was manufactured with a size of 13 x 11 UCs. Figure 13 presents the top and bottom views of the absorber. All the UCs are placed on one substrate and connected via. The back of the absorber includes microstrip lines that connect all UCs to the output port. The diameter of the via is 0.3 mm, which is not enough for successful electrochemical deposition with copper. Due to this issue, almost every UC had no connection with the microstrip lines. To overcome this problem, use specific electrically conductive glue. After applying glue and waiting for one day, the connection between the top and bottom layers of copper was established. Furthermore, the SMA port was soldered to the microstrip line. The one pin was soldered to the main line, and the ground was connected to the metal layer between the two substrates. The 2.9 mm SMA port was used as it is the most common for RF cables.

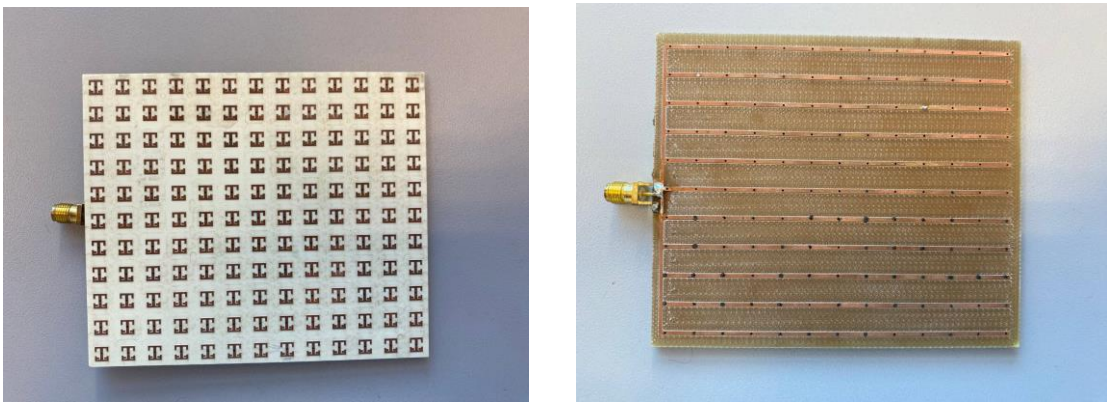

(a) (b)

Figure 13. The manufactured MTM absorber: (a) top, (b) bottom views.

Chapter 3 – Experimental setup preparation

3.1 Experimantal setup

The manufactured MTM absorber must be experimentally verified by comparing it with the simulation results. The size of the array was chosen according to the beamwidth of a wave coming from a horn antenna. The CST Simulator excites plain waves from the ports, so during the experiment, the antenna and absorber should have a certain distance between each other. The distance at which a wave emitted from an antenna becomes a plane wave can be estimated using the Fraunhofer distance formula.

$$d = \frac{2*D^2}{\lambda}, \tag{7}$$

Where d is the distance where a plane wave starts to appear, D is the highest size parameter of the antenna; in this case, it was the diameter, and λ is the wavelength.

The equation 7 was used to calculate the distance at which a wave becomes plain and resulted in 30 cm, as presented in Figure 14. After calculating the distance of the absorber from the antenna, it is important to determine the coverage area of the signal at that distance. Then, the beamwidth of the antenna wave was calculated at a distance of 30 cm, and the array size was chosen to fit the whole wave. Then, the SMA port on the absorber is connected to the spectrum analyzer to see the efficiency of the absorber. To evaluate the performance of the absorber, the gain of the antenna should be considered in the calculation. The Friis transmission equation was used to calculate the initial power ($P_{incident}$) coming from the horn antenna [18].

$$P_{incident} = P_t G_t \left(\frac{S_e}{4\pi R^2}\right), \tag{8}$$

where P_t is the amount of power applied to the antenna, G_t is the gain of the antenna, S_e is the operational surface area, and R is the distance between the antenna and absorber. The structure presented in Figure 15 was manufactured using a 3D printer to hold the MTM absorber above the

antenna. The distance between the lower and upper parts is also important, as the distance between the antenna and array should be 30 cm. The gap in the upper part is made to connect the cable from the spectrum analyzer to the output port of the MTM absorber, as presented in Figure 16. The setup will include a 3D-printed structure, anechoic chamber, signal generator, horn antenna, multimeter, and a MTM absober array. The signal generator and horn antenna LB-28-20 will be used to create incident waves.

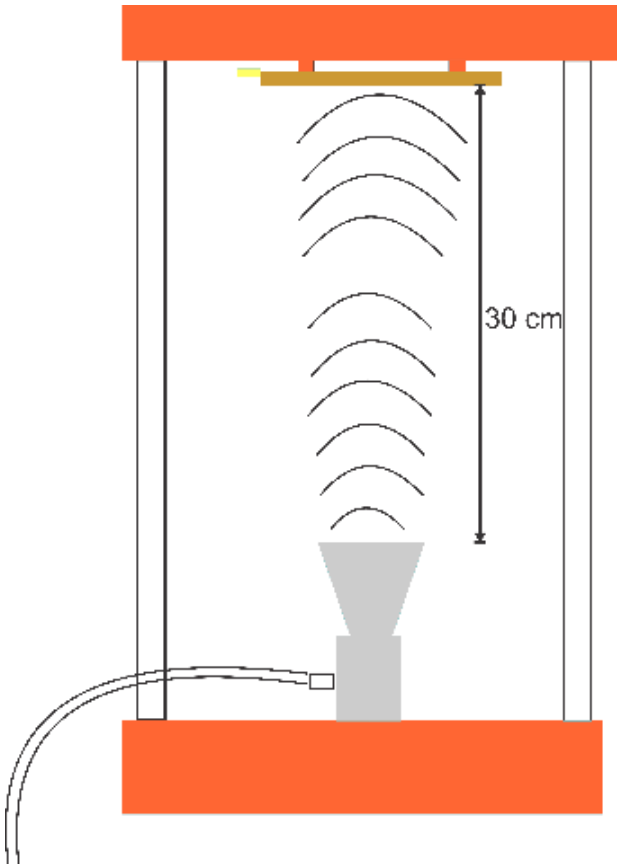

Figure 14. The diagram of the 3D printed stand with antenna and absorber.

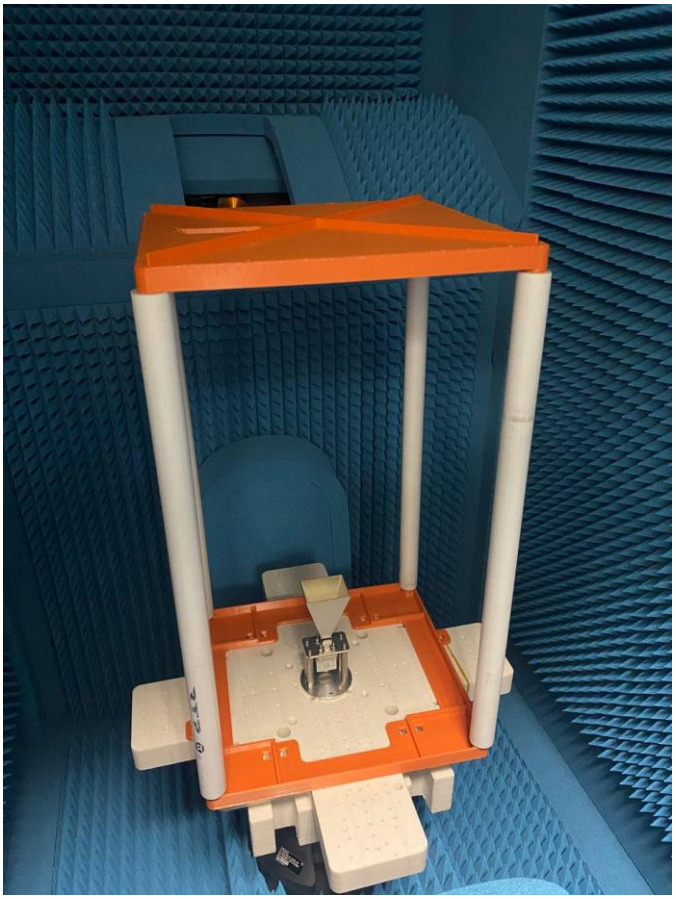

Figure 15. 3D-printed model for experimental setup.

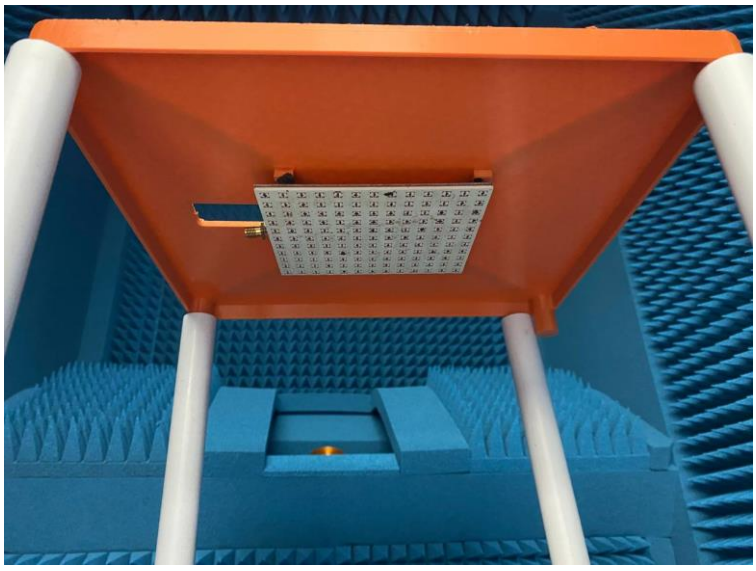

Figure 16. The upper part of the 3D model with MTM absorber.

The anechoic chamber was used to conduct the experiment with a low level of noise. The waveguides of the chamber were opened to pass the cables to the antenna and SMA port. The spectrum analyzer was chosen over a power meter to measure the gain due to the availability of the instrument and precise measurements. The two devices have different methods of measuring power; the spectrum analyzer will measure a defined span of frequency, while the power meter will measure total power, including noise. A power meter also requires an additional power sensor to operate. Two cables were used to connect the signal generator to the horna antenna, and two cables were used between the absorber SMA port and the spectrum analyzer.

The LBP 28-20 horn antenna presented in Figure 17 was used as it was available and has a stand that was designed to be used in an anchoic chamber. The size of the antenna is 40.4 mm × 33 mm × 94 mm. The following antenna operates between 26.5 GHz and 40 GHz. This is one of the reasons why the proposed absorber needed to work beyond 26.5 GHz.

Figure 17. LBP 28-20 horn antenna.

3.2 Power budjet

The power budjet is the crucial part of the experiment, as it is needed to keep devices safe and estimate the output power at each connection of the RF system. The signal generator is connected to the horn antenna using two cables, as depicted in Figure. The approximate power loss of these cables is around 0.5 dB. The horn antenna gain at the operating frequency is 19.5 dB. The free space loss between the horn antenna and the MTM absorber is 51.44 dB, which can be calculated using the equation below:

$$FSPL = 20log_{10}\left(\frac{4\pi R}{\lambda}\right) \quad (9)$$

The results of the spectrum analyzer showed -84 dB power from the SMA port.

The efficiency while transmitting a -5 dB signal from the generator was low at the operating frequency. There was around 45 dB loss from the absorption of the absorber to the spectrum analyzer. Even considering the loss of the cables and adaptors, the power loss is too high to consider the absorption to be sufficient. For further investigation, frequencies near the designed operating frequency were also measured. Power losses at different frequencies are presented in Table 1. The power loss budget was estimated by analyzing the RF circuit in Figure 17. The input power limits of the devices were considered, and it was decided to provide -5 dB of power from the signal generator. The horn antenna gain was taken from the datasheet.

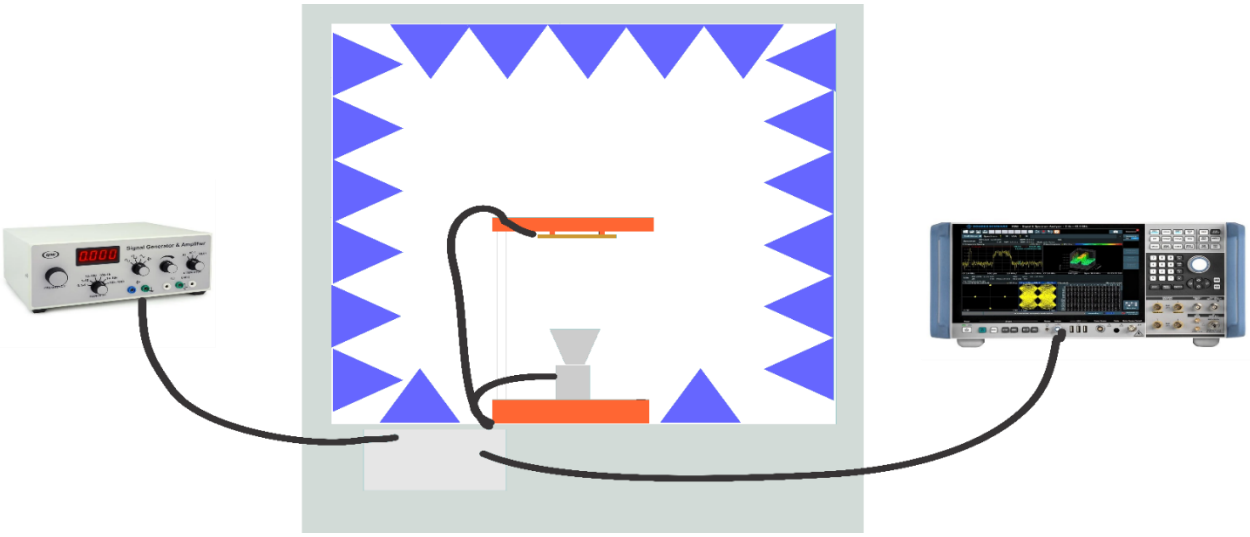

Figure 18. The RF circuit diagram for power budjet calculation.

Table 1. Power budjet of RF system.

Frequency (GHz)	Signal generator input (dB)	Cable loss (dB)	Horn antenna gain (dB)	FSPL (dB)	Cable loss (dB)
-26.5	-5	-1	18.9	-50.44	-1
-26.75	-5	-1	18.9	-50.52	-1
-27.0	-5	-1	18.9	-50.61	-1
-27.25	-5	-1	18.9	-50.69	-1
-27.5	-5	-1	19.0	-50.76	-1
-27.75	-5	-1	19.0	-50.84	-1
-28.0	-5	-1	19.1	-50.92	-1
-28.25	-5	-1	19.2	-51.01	-1
-28.5	-5	-1	19.3	-51.07	-1
-28.75	-5	-1	19.4	-51.15	-1

-29.0	-5	-1	19.5	-51.22	-1
-29.25	-5	-1	19.4	-51.30	-1
-29.5	-5	-1	19.4	-51.37	-1
-29.75	-5	-1	19.5	-51.45	-1
-30.0	-5	-1	19.6	-51.52	-1
-30.25	-5	-1	19.6	-51.59	-1
-30.5	-5	-1	19.6	-51.66	-1
-30.75	-5	-1	19.7	-51.73	-1
-31.0	-5	-1	19.8	-51.81	-1
-31.25	-5	-1	19,8	-51.88	-1
-31.5	-5	-1	19.8	-51.95	-1
-31.75	-5	-1	19.9	-52.01	-1
-32.0	-5	-1	20.0	-52.08	-1
-32.25	-5	-1	20.0	-52.15	-1
-32.5	-5	-1	20.0	-52.21	-1
-32.75	-5	-1	20.1	-52.28	-1
-33.0	-5	-1	20.1	-52.35	-1
-33.25	-5	-1	20.1	-52.41	-1
-33.5	-5	-1	20.2	-52.48	-1
-33.75	-5	-1	20.3	-52.54	-1
-34.0	-5	-1	20.3	-52.61	-1
-34.25	-5	-1	20.4	-52.67	-1
-34.5	-5	-1	20.4	-52.74	-1

-34.75	-5	-1	20.4	-52.79	-1
-35.0	-5	-1	20.4	-52.86	-1

The experiment was started by turning on the signal generator and spectrum analyzer. After connecting cables to the signal generator, the additional waveguide of the anechoic chamber was unscrewed to get the cables in. After connecting the horn antenna, the cables were connected between the absorber's SMA port and the input of the spectrum analyzer using the same waveguide. The signal generator can only provide the signal at one frequency. The spectrum analyzer and signal generator were connected to each other and controlled by different software, so measurements were done iteratively. The starting frequency was 26.5 GHz, as it is the lowest frequency supported by the horn antenna. The measurements were done until 35 GHz, with a step of 0.25 GHz and presented in Figure 18. The anechoic chamber was turned on during the experiment as it provides low-noise conditions in an active state. The 3D stand was placed on the platform of the anechoic chamber and supported with rubber bands.

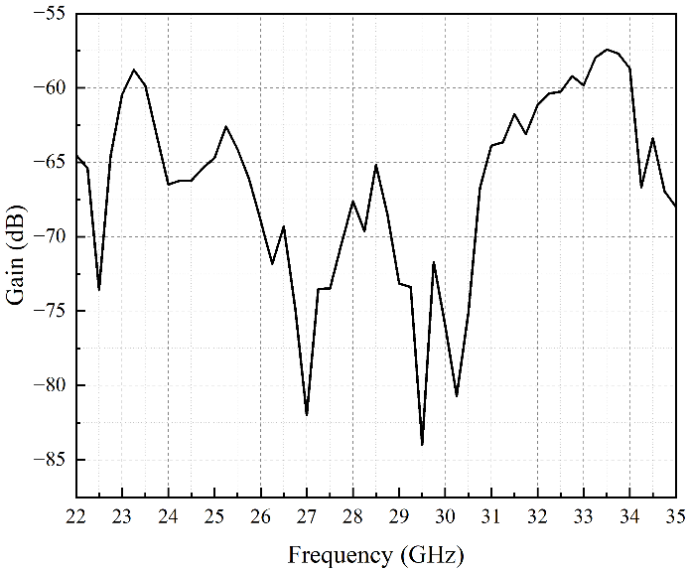

Figure 19. The results from the spectrum analyzer.

Table 2. The results of the experimental verification.

Frequency (GHz)	Power at the surface of the MTM absorber (dB)	Spectrum analyzer output (dBm)
-26.5	-38.5447	-69.3
-26.75	-38.6263	-74.81
-27.0	-38.7071	-82.0
-27.25	-38.7871	-73.5
-27.5	-38.7664	-73.48
-27.75	-38.8451	-70.46
-28.0	-38.823	-67.61
-28.25	-38.8002	-69.62
-28.5	-38.7767	-65.17
-28.75	-38.7525	-68.5
-29.0	-38.7278	-73.14
-29.25	-38.9023	-73.37
-29.5	-38.9762	-84.0
-29.75	-38.9495	-71.69
-30.0	-38.9222	-75.95
-30.25	-38.9943	-80.7
-30.5	-39.0658	-75.09
-30.75	-39.0367	-66.72
-31.0	-39.007	-63.87
-31.25	-39.0768	-63.66

-31.5	-39.146	-61.76
-31.75	-39.1147	-63.11
-32.0	-39.0828	-61.13
-32.25	-39.1504	-60.39
-32.5	-39.2175	-60.26
-32.75	-39.184	-59.2
-33.0	-39.2501	-59.83
-33.25	-39.3156	-57.97
-33.5	-39.2807	-57.42
-33.75	-39.2453	-57.7
-34.0	-39.3094	-58.7
-34.25	-39.273	-66.67
-34.5	-39.3362	-63.38
-34.75	-39.3989	-66.95
-35.0	-39.4612	-68.0

The experimental measurements showed that the highest power was obtained not at the designed frequency but at -33.5 GHz. The spectrum analyzer showed -57.42 dBm power, while the power coming towards the MTM antenna was expected to be -39.2807 dB. There was still a difference of -17.14 dB if the cable loss between the spectrum analyzer and the device under the test was subtracted. For further investigation of the problem, the vector network analyzer was used to verify the impedance matching of the output port. The vector network analyzer was turned on, and the E-calibration module was connected to it. The calibration was done on the single input port,

as there is only one output SMA port on the absorber. The absorber was connected to the cable of the vector network analyzer using a 2.4 mm to 2.9 mm adaptor. The results of the vector network analyzer are presented as a graph. The graph didn’t go lower than -10 dB at the operating frequency, which meant a poor impedance match.

Chapter 4 – Discussion

In discussing the benefits and drawbacks of employing solar energy for indoor energy collection, the thesis points out that although solar panels provide a sustainable energy source, their efficiency is constrained indoors by lower light levels and spatial limitations. On the other hand, mechanical vibrations offer a viable substitute, particularly in interior spaces with heavy traffic. The study analyze the idea of piezoelectric disks, which provide a dependable and low-maintenance power source for wireless communication devices by converting mechanical strain into electrical energy.

A large portion of the study is focused on RF energy harvesting, which works especially well inside where there are a lot of RF sources. In this context, the paper examines the potential of MTM absorbers and emphasizes their near-perfect electromagnetic wave absorption capabilities. The design and simulation of a special UC absorber, the foundation of an MTM absorber array, are presented in the thesis. The step-by-step design construction was used and split-ring-reonator taken as a fundamental design. The efficiency of the suggested design is confirmed by the high absorption rate shown in the simulation results in CST Simulator.

The process of developing and testing the MTM absorber array is described in depth in the sections on experimental setup and method development. The MTM array was also simulated to examine the frequency shift and absorption rate changes. The optimization of the microstrip lines at the back of the absorber provided the impedance match. The study highlights how crucial it is to have a carefully thought-out experimental setup to determine the effectiveness of the absorber. The setuo includes an anechoic chamber, a spectrum analyzer, a horn antenna, RF cables, and a 3D-printed absorber-holding framework. The distance between the absorber and antenna was also calculated to have a plane wave effect. The power budget of the RF circuit was calculated to

estimate the output power and guarantee the device's safety during the experiment. The iterative measurements showed that the absorption is low at 29.5 GHz. The other frequencies were also measured, and absorption at -33.5 GHz was the highest among them all. The frequency shift may be the result of soldering the SMA port and the microstrip line defects during manufacturing, which led to the poor impedance match. The impedance match was tested using a vector network analyzer and showed a low impedance match at operating frequency.

Overall, the thesis needs further experimental validation and comparison with simulation results. There are some difficulties with the impedance matching of the SMA port that can be solved by finding an equivalent circuit for the design and implementing matching elements. The future work should concentrate on increasing the absorption and frequency range.

Chapter 5 – Conclusion

The thesis work was focused on RF energy harvesting using MTM absorbers. The literature review showed the potential of MTM-based absorbers in wireless communication networks for powering devices. However, the RF energy harvesting may not be enough, so other harvesting methods should also be implemented to create a sustainable communication system. The experimental results showed -58 dBm gain at 30 GHz, which is slightly off from the operating frequency. This problem should be addressed by impedance matching the port and MTM absorber. This will give us the opportunity to analyze only the absorption power of the proposed design.

References

[1] Z. Zheng et al., “A Wireless Power Transfer System Based on Dual-Band Metamaterials,” in *IEEE Microwave and Wireless Components Letters*, vol. 32, no. 6, pp. 615-618, June 2022.

[2] Swapnil Bawankar, et al., “Environmental impact assessment of lithium ion battery employing cradle to grave,” *Sustainable Energy Technologies and Assessments*, Volume 60,2023, 103530, ISSN 2213-1388.

[3] W. Gao, et al., “Efficient all-small-molecule organic solar cells processed with non-halogen solvent,” *Nature Communications*, vol. 15 (1), art. no. 1946, 2024.

[4] L. Kaixing, et al., “A hybrid energy supply system based on metamaterial antenna integrated solar cells for IoT nodes,” *Sustainable Energy Technologies and Assessments*, 64, art. no. 103678, 2024.

[5] X. Xiangming, and X. Li. “Asymptotic Analysis of Radial Vibration of Thin Piezoelectric Disks.” *Journal of the American Ceramic Society* vol. 104.7: 3411–3423, 2021.

[6] Erturk, Alper., and D. J. Inman. Piezoelectric Energy Harvesting. Chichester: Wiley, 2011. Print.

[7] Khan, Taimoor, Nasimuddin, and Yahia Antar. Elements of Radio Frequency Energy Harvesting and Wireless Power Transfer Systems. First edition. Boca Raton, FL: CRC Press, 2021.

[8] Iannacci, Jacopo. “Internet of Things (IoT); Internet of Everything (IoE); Tactile Internet; 5G – A (Not so Evanescent) Unifying Vision Empowered by EH-MEMS (Energy Harvesting MEMS) and RF-MEMS (Radio Frequency MEMS).” *Sensors and actuators. A. Physical*. 272 (2018): 187–198.

[9] Singh, Amit Kumar, Shiban K. Koul, and Mahesh Abegaonkar. Metamaterials for Antenna Applications. Boca Raton, FL: CRC Press, 2022. Print.

[10] S. Mahlknecht and M. Roetzer, "Energy supply considerations for self-sustaining wireless sensor networks," *Proceeedings of the Second European Workshop on Wireless Sensor Networks*, 2005., Istanbul, Turkey, 2005, pp. 397-399, doi: 10.1109/EWSN.2005.1462032.

[11] X. Lu, P. Wang, D. Niyato, D. I. Kim and Z. Han, "Wireless Charging Technologies: Fundamentals, Standards, and Network Applications," *in IEEE Communications Surveys & Tutorials*, vol. 18, no. 2, pp. 1413-1452, Secondquarter 2016, doi: 10.1109/COMST.2015.2499783.

[12] S. Kim et al., "Ambient RF Energy-Harvesting Technologies for Self-Sustainable Standalone Wireless Sensor Platforms," *in Proceedings of the IEEE*, vol. 102, no. 11, pp. 1649-1666, Nov. 2014, doi: 10.1109/JPROC.2014.2357031.

[13] F. Ye, Y. Qian and R. Q. Hu, "Energy Efficient Self-Sustaining Wireless Neighborhood Area Network Design for Smart Grid," *in IEEE Transactions on Smart Grid*, vol. 6, no. 1, pp. 220-229, Jan. 2015, doi: 10.1109/TSG.2014.2344659.

[14] P. N. Alevizos and A. Bletsas, "Sensitive and Nonlinear Far-Field RF Energy Harvesting in Wireless Communications," *in IEEE Transactions on Wireless Communications*, vol. 17, no. 6, pp. 3670-3685, June 2018, doi: 10.1109/TWC.2018.2812889.

[15] X. Chen et al., “Robust Method to Retrieve the Constitutive Effective Parameters of Metamaterials,” *Physical Review E Covering Statistical, Nonlinear, Biological, and Soft Matter Physics*, vol. 70, no. 12, pp. 1-7, Jul. 2004.

[16] O. Hema et al., “New compact six-band metamaterial absorber based on Closed Circular Ring Resonator (CCRR) for Radar applications,” *Optics Communications*, vol. 503, 2022.

[17] X. Du et. al., “A Broadband Switchable Metamaterial Absorber/Reflector Based On Multi-Laps Graphene Sheets in the Terahertz Band,” *in IEEE Photonics Journal*, vol. 13, no. 5, pp. 1-8, Oct. 2021.

[18] M. Karaaslan, et. al, “Microwave energy harvesting based on metamaterial absorbers with multi-layered square split rings for wireless communications,” *Optics Communications*, vol. 392, 2017, pp 31-38, ISSN 0030-4018,

[19] G.P.E. Persis, et al., “A compact tilted split ring multiband metamaterial absorber for energy harvesting applications,” *Materials Today: Proceedings*, vol. 56, part 1, pp. 368-372, 2022.

[20] C. Fowler, et al., “High efficiency ambient RF energy harvesting by a metamaterial perfect absorber,” *Opt. Mater. Express* vol. 12, 1242-1250, 2022.

[21] M. Amin, et al., “An Interference-Based Quadruple-L Cross Metasurface Absorber for RF Energy Harvesting,” *IEEE Antennas and Wireless Propagation Letters*, vol. 20, no. 10, pp. 2043-2047, Oct. 2021.

[22] K. Muharrem, et al., “Microwave energy harvesting based on metamaterial absorbers with multi-layered square split rings for wireless communications, ” *Optics Communications*, vol. 392, pp. 31-38, ISSN 0030-4018, 2017.

[23] Zolfaghary pour, S., Chegini, E., Mighani, M., “Design of wideband metamaterial absorber using circuit theory for X-band applications,” *IET Microw. Antennas Propag*. 17(4), 292–300, 2023.

[24] Kaur KP, et.al., “Ultrathin dual-layer triple-band flexible microwave metamaterial absorber for energy harvesting applications,” *Int J RF Microw Comput Aided Eng*. 2019; 29:e21646.

[25] Al-Bawril, Samir Salem, and Mohammad Tariqul Islam. “Metamaterial for Future Generation Wireless Communications.” Metamaterial for Microwave Applications. 1st ed. Vol. 1. CRC Press, 2023. 65–92.

[26] W. Dongxu, et. al., “A High Q-Factor Dual-Band Terahertz Metamaterial Absorber and Its Sensing Characteristics,” *Nanoscale*, 2023, 15. 10.1039/D2NR05820K.

[17] Chen, X. et al., “Robust method to retrieve the constitutive effective parameters of metamaterials,” *Physical Review E - Statistical, Nonlinear, and Soft Matter Physics*, v. 70, n. 1 2, p. 016608-1-016608-7, July, 2004.

[18] N. Ullah, et al., “A compact-sized four-band metamaterial-based perfect absorber for electromagnetic energy harvesting applications,” *Optics & Laser Technology*, vol. 168, 109836, 2024.